Int J Adv Manuf Technol (2016) 87:3373–3388
DOI 10.1007/s00170-016-8671-8

ORIGINAL ARTICLE

An efficient approach for milling dynamics modeling and analysis with varying time delay and cutter runout effect

Xing Zhang[1] · Jun Zhang[1] · Bo Pang[1] · DiaoDiao Wu[1] · XiaoWei Zheng[2] · WanHua Zhao[1]

Received: 21 December 2015 / Accepted: 23 March 2016 / Published online: 14 April 2016

Abstract An efficient approach for milling stability and surface location error (SLE) prediction with varying time delay and cutter runout effect is presented in this paper. Firstly, based on the tooth trochoid motion, the paper proposes a varying time delay model during cutter/workpiece engagement with taking cutter runout into account, establishes a milling dynamic model under arbitrary feed direction, and then derives the state transition matrix in one cutter rotation period by using the Cotes numerical integration formula. The milling stability of the dynamics system are obtained by using Floquet theory. According to the fixed point theory, the displacement response of the dynamic system and the method for solving the SLE are both developed. Later, a series of numerical and experimental works are conducted. The numerical verification shows that the proposed method can achieve a faster convergence rate and higher calculation efficiency than other previous methods. Meanwhile, the prediction of stability and SLE are in good agreement with the experimental results, and have a high accuracy for stability prediction when cutter runout and varying time delay considered. In the end, the numerical studies show that the milling stability and SLE strongly depends on the actual milling conditions, including milling parameters, cutter runout, cutter geometric parameters, and asymmetric structural dynamic parameters, which are helpful for milling process optimization.

Keywords Milling stability · SLE · Varying time delay · Cutter runout · Cotes numerical integration formula · Asymmetric structure

Nomenclature

XYZ	Global coordinate system
$X_r Y_r Z_r$	Tool rotation coordinate system
$X_f Y_f Z_f$	Local feed coordinate system
ψ	Feed directional angle
R	Nominal tool radius
ρ, λ	Cutter runout value and angle
$\varphi_{i,j}(t)$	Rotation angle of the jth axial disk element on the ith tooth
$\tau_{i,j}(t)$	Time delay item of jth cutting disk element on ith tooth at moment
$h_{i,j}(t)$	Instantaneous uncut chip thickness of jth cutting disk element on ith tooth at moment
$m_x, m_y, c_x, c_y, k_x, k_y$	Modal mass, damping and stiffness in the and directions
$\bar{\tau}(t)$	Average time delay for all in-cut tooth at moment
k_t, k_r	Shearing specific cutting force coefficient in tangential and radial direction
n, aD, a_p, f_t	Spindle speed, radial immersion ratio, axial depth of cut, and feed per tooth
m	Discretized time intervals
Φ	System transition matrix
SLE	Surface location error

✉ WanHua Zhao
whzhao@mail.xjtu.edu.cn

[1] State Key Laboratory for Manufacturing Systems Engineering, Xi'an Jiaotong University, Xi'an, Shaanxi 710054, China

[2] Aviation Industry Corporation of China, Xi'an Aircraft Industry (Group) Company LTD, Xi'an, Shaanxi 710054, China

1 Introduction

High efficiency and accuracy machining is the eternal goal for manufacturing industry. Chatter and resonance during milling process are two main unfavorable factors for further improving machining efficiency and accuracy. Chatter is a self-excited vibration as a result of dynamical interaction between tool and workpiece, and resonance is a forced vibration coming from external incentive acting on milling system. Unless avoided, otherwise, it would lead to poor surface finish and even tool breakage. Actually, in order to obtain good processing quality, milling process should be operated under stable condition [1, 2]. Hence, evaluating if the milling parameters satisfied high-performance machining or not is becoming as a problem for manufacturer. Currently, a lot of researches have been conducted on milling stability and surface accuracy.

For milling stability, Tlusty et al. [3], Tobias [4, 5], and Merrit [6], as pioneers in the study of chatter, proposed the regeneration modulation mechanism, employed a time delay displacement variable to couple cutting force and tool dynamic response, then put forward the milling dynamic model as a delay differential equation, and finally draw a stability diagram lobe to distinguish stable and unstable regions within parameter domain. As the delay dynamics model has infinite dimensional state space, and existing mathematical method cannot obtain an analytical solution. In decades of development, researchers have developed many methods to study the stability characteristics of the differential equations for milling process. Early, Tlusty and Ismail [7, 8] numerically investigated the stability prediction through direct time domain simulation of dynamic response, but the calculation process is time consuming. For frequency domain methods, Altintas et al. [9, 10] developed the ZOA method to calculate stability diagram analytically. The calculation speed is very fast, but the high order harmonics of periodic direction matrix are ignored, which results in a poor prediction accuracy, especially under the low radial immersion milling condition. Then, Merdol and Altintas [11] expanded their research work and proposed a multi-frequency method, in which the high order expansion of the direction matrix is considered, but an iterative search process for chatter frequency is needed. For the differential equation based methods, Insperger and Stépán [12] operated time delay item in delay differential equation by zero order discretization processing, then transformed the dynamics equation to a series of ordinary differential equations, proposed the semi-discretization method for stability prediction. Later, Insperger and Stépán [13] proposed the first-order semi-discretization method to improve the accuracy of the algorithm. Different from the semi-discretization method, Ding et al. [14] discretized both the time delay item and state item, and proposed the full-discretization method. Subsequently, Ding et al. [15] and Quo et al. [16] further proposed the second and third-discretization methods. Besides, Ding et al. [17] and Zhang et al. [18] considered the state equation as an initial value problem of differential equation, and used numerical integration method to obtain milling stability.

It is worth noting that all above works are studied under the assumption with only one constant time delay in the milling dynamics equation. This constant time delay is equal to the tooth passing period. Actually, the tooth motion trajectory is a trochoidal equation [19], the time delay is related to the milling parameters and the cutter geometric parameters, and is a periodic time varying variable. When considering the tooth motion, Long et al. [20] pointed out the feed velocity would affect the time delay, especially during the tooth entry/exit stage, and then proposed a varying time delay milling dynamics model to analyze the influence of feed velocity on milling stability. Based on Balachandran's model, Song et al. [21] studied the stability during micro-milling process. For the varying time delay milling dynamics model, the calculation time for state transition matrix is too long. In order to improve calculation efficiency, an equivalent time delay was used to reflect the varying time delay effect caused by the motion of tool and obtain a high efficiency algorithm for stability prediction during 5-axis ball-end milling process [22]. Additionally, Seguy et al. [23] studied the stability of multi-time delay milling system with spindle speed variation, and Sellmeier et al. [24] analyzed the influence of multi-time delay on milling stability using non-constant pitch cutter. What should be noted is that these studies have not considered the cutter runout factor. Cutter runout would result in the changes of real cutting radius, so the current tooth maybe cut the workpiece which is left by several previous tooth. At this point, the time delay between the teeth is no longer the same, and its revolution will be equal to the tool rotation period, no longer the tooth passing period. Wan et al. [25] demonstrated an improved version of semi-discretization method, in which the influence of multiple time delays caused by cutter runout and nonconstant pitch cutter on milling stability is considered. But the method does not consider the periodical variant characteristics of the time delay.

Once the milling process is stable, it is very important to study machining accuracy and its relationship with parameters. It is well known that the machining error of the parts is formed by the macroscopical motion of the tool relative to the workpiece superimposing the microscopical vibration of tool induced by cutting force. Considering the dynamic excitation process, Montgomery and Altintas [26] analyzed generation process of machined surface based on mechanistic cutting force model. Later, Altintas et al. [27, 28] further analyzed the influence of cutter runout and dynamic response on surface topography. Ismail et al. [29] focused

on the generation of milled surfaces with cutter runout, vibration and flank wear effects. Schmitz et al. [30] used the surface location error (SLE) to describe the machining precision, and analyzed the surface roughness and SLE with different milling parameters through simulation cases. Later, Schmitz [31] proposed a numerical method for the surface generation, but this method is time consuming and is not conducive to the rapid calculation of SLE. Recently, Surmann et al. [32, 33] have proposed an approach to predict the surface topography by considering the vibration of cutter, but without cutter runout. It can be seen that SLE is an effective index to characterize the machining errors, but at present, the research on SLE with taking tooth trochoid motion and cutter runout into account is relatively little.

The above literature review indicates that the current lack of comprehensive consideration of time varying delay and cutter runout on the milling stability, and the influence of cutter runout on SLE is also relatively short. Because of the complexity of the state transformation matrix for the varying time delay dynamics system, the stability analysis is much time consuming. This paper adopts the mean value of the varying time delay to reflect its time varying effect. Based on a high order accuracy of the numerical integration formula, the paper presents an efficient method to predict the stability and SLE during milling process with the consideration of tooth trochoid motion and cutter runout effect. The main content of this paper is as follows: following the introduction, Section 2 firstly presents a periodic varying time delay model considering the tooth trochoid motion and cutter runout effect. Based on the Cotes numerical integration formula, the paper further gives an efficient method for milling stability and SLE. Section 3 firstly illustrates the efficiency of stability prediction without cutter runout, and then examine the prediction accuracy with cutter runout through experiments. Section 4 numerically studies the influence of milling parameters, cutter runout parameters, cutter geometry parameters, and asymmetric structure dynamics parameters on milling stability and SLE. Finally, the presented study is summarized in the conclusions.

2 Milling dynamics analysis

2.1 Cutter/workpiece engagement with cutter runout effect

A general milling process is shown in Fig. 1a. In order to describe the tool motion process, XYZ is defined as the global stationary coordinate system attached to the worktable where the workpiece geometry boundary and tool path are described. $X_r Y_r Z_r$ is created as the tool rotation coordinate system attached to the tool system with its origin fixed at the tool center point and only do translational motion

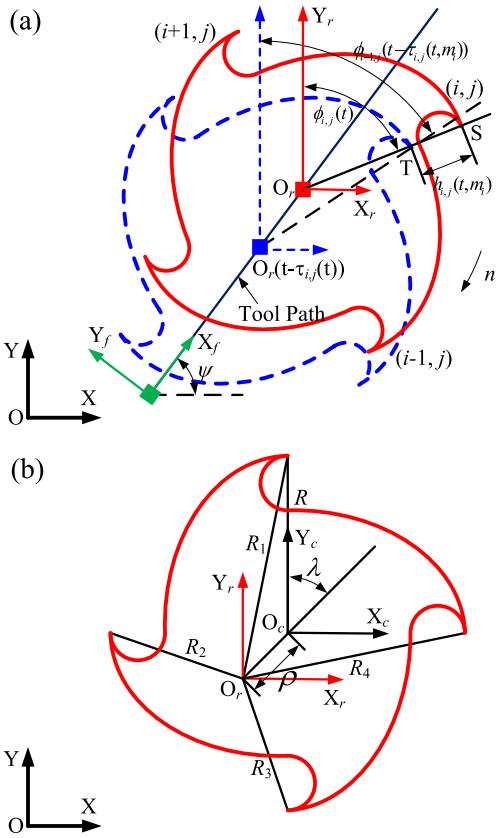

Fig. 1 General milling process. **a** Cutter motion process. **b** Tool geometry with cutter runout

relative to XYZ. $X_f Y_f Z_f$ is the local feed coordinate system. X_f is aligned with the feed direction of the theoretical tool path and the angle between X_f and X is ψ. Cutter runout is quite common in machining process, which can be described by the runout value ρ and runout angle λ as shown in Fig. 1b. To conveniently describe the cutter/workpiece engagement process, the axial cutting part of the tool is divided into N_a disk elements with an equivalent axial length along the tool axis. As shown in Fig. 1a, since several teeth may fail cut workpiece due to cutter runout, the instantaneous uncut chip thickness $h_{i,j}(t, m_i)$ for the current cutting point is the distance between point S and the point T with the same position angle of previous m_ith tooth.

With consideration of cutter runout effect, the actual tooth cutting radius is

$$R_{i,j} = \sqrt{R^2 + \rho^2 - 2R\rho\cos\left(\pi - \lambda - \gamma_i^0 - (j-1)\beta_0\right)} \quad (1)$$

where R is the nominal tool radius. β_0 is the flag angle for one cutting element due to tool helix angle. $\gamma_i^0$is the nominal pitch angle between ith tooth and 1th tooth.

At time t, the current cutter position is shown as Fig. 1a. The rotation angle $\phi_{i,j}(t)$ of the jth axial disk element on the ith tooth is expressed as follows.

$$\phi_{i,j}(t) = \frac{2\pi\Omega}{60}t - \gamma_{i,j} - (j-1)\beta_0 \tag{2}$$

where Ω is the spindle speed. $\gamma_{i,j}$ is the actual pitch angle between ith tooth and 1th tooth. At this moment, the coordinate of point S in **XYZ** can be given by

$$\begin{bmatrix} S_{x,i,j} \\ S_{y,i,j} \end{bmatrix} = \begin{bmatrix} o_{rx}(t) \\ o_{ry}(t) \end{bmatrix} + \begin{bmatrix} R_{i,j}\sin(\phi_{i,j}(t)) \\ R_{i,j}\cos(\phi_{i,j}(t)) \end{bmatrix} \tag{3}$$

Similarly, at time $t - \tau_{i,j}(t, m_i)$, the coordinate of point T in **XYZ** can be given by

$$\begin{bmatrix} T_{x,i-m_i,j} \\ T_{y,i-m_i,j} \end{bmatrix} = \begin{bmatrix} o_{rx}(t-\tau_{i,j}(t,m_i)) \\ o_{ry}(t-\tau_{i,j}(t,m_i)) \end{bmatrix} + \begin{bmatrix} R_{i-m_i,j}\sin(\phi_{i-m_i}(t-\tau_{i,j}(t,m_i))) \\ R_{i-m_i,j}\cos(\phi_{i-m_i}(t-\tau_{i,j}(t,m_i))) \end{bmatrix} \tag{4}$$

Meanwhile, the coordinate of point T in **XYZ** can also be expressed as

$$\begin{bmatrix} T_{x,i-m_i,j} \\ T_{y,i-m_i,j} \end{bmatrix} = \begin{bmatrix} o_{rx}(t) \\ o_{ry}(t) \end{bmatrix} + \begin{bmatrix} (R_{i,j} - h_{i,j}(t,m_i))\sin(\phi_{i,j}(t)) \\ (R_{i,j} - h_{i,j}(t,m_i))\cos(\phi_{i,j}(t)) \end{bmatrix} \tag{5}$$

By combining Eq. 4 with Eq. 5, the following equation can be achieved.

$$\begin{bmatrix} o_{rx}(t-\tau_{i,j}(t,m_i)) \\ o_{ry}(t-\tau_{i,j}(t,m_i)) \end{bmatrix} + \begin{bmatrix} R_{i-m_i,j}\sin(\phi_{i-m_i}(t-\tau_{i,j}(t,m_i))) \\ R_{i-m_i,j}\cos(\phi_{i-m_i}(t-\tau_{i,j}(t,m_i))) \end{bmatrix} = \begin{bmatrix} o_{rx}(t) \\ o_{ry}(t) \end{bmatrix} + \begin{bmatrix} (R_{i,j} - h_{i,j}(t,m_i))\sin(\phi_{i,j}(t)) \\ (R_{i,j} - h_{i,j}(t,m_i))\cos(\phi_{i,j}(t)) \end{bmatrix} \tag{6}$$

As cutter do translational motion along X_f with a feed velocity of f_v, we can obtain Eq. 7.

$$\begin{bmatrix} o_{rx}(t) \\ o_{ry}(t) \end{bmatrix} - \begin{bmatrix} o_{rx}(t-\tau_{i,j}(t,m_i)) \\ o_{ry}(t-\tau_{i,j}(t,m_i)) \end{bmatrix} = \begin{bmatrix} \cos\psi \\ \sin\psi \end{bmatrix} f_v\tau_{i,j}(t,m_i) \tag{7}$$

Besides, the rotation angle $\phi_{i-m_i,j}(t - \tau_{i,j}(t, m_i))$ in Eq. 6 can be derived as

$$\phi_{i-m_i,j}(t-\tau_{i,j}(t,m_i)) = \phi_{i,j}(t) - \frac{2\pi\Omega}{60}\tau_{i,j}(t,m_i) + \gamma_{i,j} - \gamma_{i-m_i,j} \tag{8}$$

Owing to $\Delta = \gamma_{i,j} - \gamma_{i-m_i,j} - \frac{2\pi\Omega}{60}\tau_{i,j}(t,m_i) \approx 0$, we can employ $\sin\Delta \approx \Delta$. As a result of combining Eqs. 6–8, the time delay $\tau_{i,j}(t, m_i)$ can be determined by

$$\tau_{i,j}(t,m_i) = \frac{R_{i-m_i,j}(\gamma_{i,j} - \gamma_{i-m_i,j})}{R_{i-m_i,j}\frac{2\pi\Omega}{60} + f_v\cos(\psi + \varphi_{i,j}(t))} \tag{9}$$

Furthermore, the instantaneous uncut chip thickness $h_{i,j}(t, m_i)$ can be shown as

$$h_{i,j}(t,m_i) = \sin(\varphi_{i,j}(t)+\psi)f_v\tau_{i,j}(t,m_i) + R_{i,j} - R_{i-m_i,j}\cos\left(\frac{2\pi\Omega\tau_{i,j}(t,m_i)}{60} - \gamma_{i,j} + \gamma_{i-m_i,j}\right) \tag{10}$$

The actual instantaneous uncut chip thickness at current tooth position is the maximum between zero and the minimum of all possible chip thickness defined by Eq. 10 over $m_i = 1, 2, ..., N_t$, which is mathematically expressed by Eq. 11. Ultimately, the time delay item $\tau_{i,j}(t)$ can be determined with m_i.

$$h_{i,j}(t) = \max(0, \min(h_{i,j}(t,m_i))) \quad m_i = 1, 2, \cdots N_t \tag{11}$$

As mentioned above, it can be seen that the time delay item is a varying parameter with time, not a constant one. Here is a numerical case to address this problem clearly. Figure 2 shows the instantaneous chip thickness and time delay item during cutter/workpiece engagement of a three

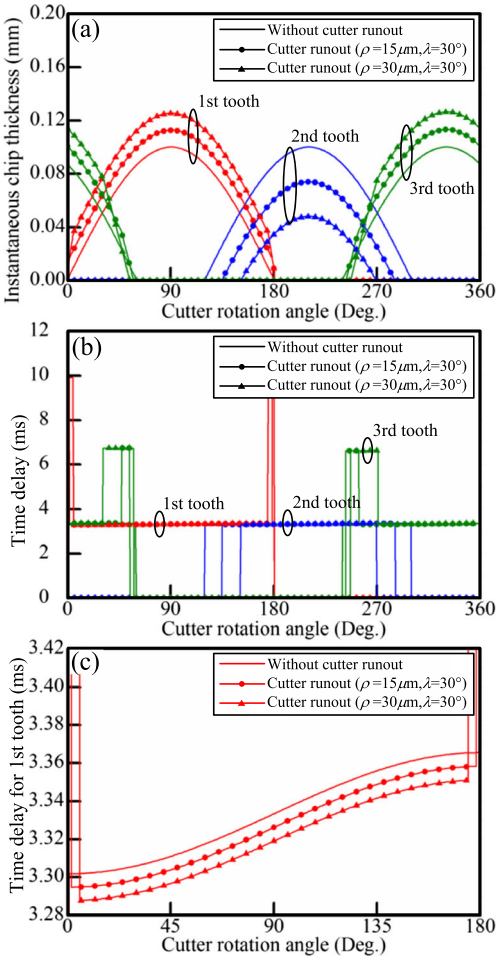

Fig. 2 Cutter/workpiece engagement with cutter runout effect, $N_t = 3$, $n = 6000$ rpm, $f_t = 0.1$ mm/tooth. **a** Instantaneous chip thickness. **b** Time delay item. **c** Time delay for 1st tooth

teeth cutter with runout effect. In this simulation for the slot milling, the spindle speed n is 6000 rpm, and the feed per tooth f_t is 0.1 mm/tooth. It can be concluded that the chip thickness and time delay item between different teeth would change evidently in the milling case with cutter runout. Due to cutter runout, tooth maybe lost of cut at some local cutter rotation angle, as a result, the delay time for other tooth would change suddenly as shown in Fig. 2b. Furthermore, from Fig. 2c, we can know that the time delay for one fixed tooth is also changeable at different angle position. Obviously, the time delay of the proposed method is less than the traditional constant one when cutter rotation angle is under than 90°, but greater when cutter rotation angle is upper than 90°.

2.2 Milling dynamics model

Generally, the cutter is assumed flexible while the workpiece is considered rigid in the 2-DOF milling dynamics model, the dynamic system of the machine tool with regenerative effect can be expressed by a n-dimensional linear non-autonomous DDE model

$$\mathbf{M}\ddot{\mathbf{q}}(t)+\mathbf{C}\ddot{\mathbf{q}}(t)+\mathbf{K}\mathbf{q}(t)=\mathbf{K_c}(t)[\mathbf{q}(t-\bar{\tau}(t))-\mathbf{q}(t)]+\mathbf{F}(t)$$
$$\text{where } \mathbf{M}=\begin{bmatrix} m_x & 0 \\ 0 & m_y \end{bmatrix}, \mathbf{C}=\begin{bmatrix} c_x & 0 \\ 0 & c_y \end{bmatrix}, \mathbf{K}=\begin{bmatrix} k_x & 0 \\ 0 & k_y \end{bmatrix} \quad (12)$$

with m_x, m_y, c_x, c_y, k_x, and k_y denote the modal mass, damping and stiffness in the X and Y directions, respectively. $\mathbf{q}=[x, y]^T$ denotes the displacement vector. $\bar{\tau}(t)$ is the average time delay for all in-cut tooth which can be derived as (Fig. 3)

$$\bar{\tau}(t)=\frac{1}{N_a N_t}\sum_i\sum_j \tau_{i,j}(t) \quad (13)$$

In Eq. 12, $\mathbf{K_c}(t)[\mathbf{q}(t-\bar{\tau}(t))-\mathbf{q}(t)]$ represents the regenerative effect item, in which $\mathbf{K_c}(t)$ denotes the directional cutting force coefficient matrix expressed as follows.

$$\mathbf{K_c}(t)=db\sum_i\sum_j g(\phi_{i,j}(t))\begin{bmatrix} -k_t\sin(\phi_{i,j})\cos(\varphi_{i,j})-k_r\sin(\phi_{i,j})^2 & -k_t\cos(\phi_{i,j})^2-k_r\sin(\phi_{i,j})\cos(\phi_{i,j}) \\ k_t\sin(\phi_{i,j})^2-k_r\sin(\phi_{i,j})\cos(\phi_{i,j}) & k_t\sin(\phi_{i,j})\cos(\phi_{i,j})-k_r\cos(\phi_{i,j})^2 \end{bmatrix} \quad (14)$$

where k_t and k_r are the tangential and the normal specific cutting force coefficients, respectively. The window function $g(\phi_i(t))$ is defined as

$$g(\phi_i(t))=\begin{cases} 1 & if\ \theta_{en}<\phi_{i,j}<\theta_{ex} \\ 0 & otherwise \end{cases} \quad (15)$$

where θ_{st} and θ_{ex} are the entry and exit angles of the jth cutting element of the ith cutter tooth, respectively.

$\mathbf{F}(t)=[F_x, F_y]^T$ represents the nominal cutting forces, which can be expressed as

$$\mathbf{F}(t)=db\sum_i\sum_j g(\phi_{i,j}(t))\begin{bmatrix} -k_t\cos(\phi_{i,j})-k_r\sin(\phi_{i,j}) \\ k_t\sin(\phi_{i,j})-k_r\cos(\phi_{i,j}) \end{bmatrix} h_{i,j}(t) \quad (16)$$

2.3 Efficient method for milling stability and SLE prediction

With the aid of state space theory, let $\mathbf{P}(t)=\mathbf{M}\dot{\mathbf{q}}+\mathbf{C}\mathbf{q}/2$, set state item $\mathbf{X}(t)=[\mathbf{q}(t)\quad \mathbf{P}(t)]^T$, Eq. 12 can be transformed into

$$\dot{\mathbf{X}}(t)=\mathbf{A}\mathbf{X}(t)+\mathbf{B}(t)[\mathbf{X}(t-\bar{\tau}(t))-\mathbf{X}(t)]+\mathbf{C}(t)$$
$$\text{where } \mathbf{A}=\begin{bmatrix} -\mathbf{M}^{-1}\mathbf{C}/2 & \mathbf{M}^{-1} \\ \mathbf{C}\mathbf{M}^{-1}\mathbf{C}/4-\mathbf{K} & -\mathbf{C}\mathbf{M}^{-1}/2 \end{bmatrix}$$
$$\mathbf{B}(t)=\begin{bmatrix} \mathbf{0} & \mathbf{0} \\ \mathbf{K_c}(t) & \mathbf{0} \end{bmatrix}$$
$$\mathbf{C}(t)=\begin{bmatrix} \mathbf{0} \\ \mathbf{F}(t) \end{bmatrix} \quad (17)$$

In above equation, $\mathbf{A}$ is a constant matrix standing for the time invariants of the milling dynamic system. $\mathbf{B}(t)$ and $\mathbf{C}(t)$ are periodic matrixes with the spindle rotation period T. In order to obtain the stability lobes of the dynamic system, the first step is to divide T into m time intervals, i.e., $T=m\tau$. Now, the discretized time point is

$$t_k=t_1+(k-1)\tau \quad (k=1, 2, ..., m+1) \quad (18)$$

Then, the response of Eq. 17 can be solved as an initial value problem

$$\mathbf{X}(t)=\mathbf{X}(t_k)+\int_{t_k}^{t}\mathbf{G}(t)dt \quad (19)$$

where $\mathbf{G}(t)=\mathbf{F}(t)\mathbf{X}(t)+\mathbf{B}(t)\mathbf{X}(t-\bar{\tau}(t))+\mathbf{C}(t)$ with $\mathbf{F}(t)=\mathbf{A}-\mathbf{B}(t)$. As a numerical integration method,

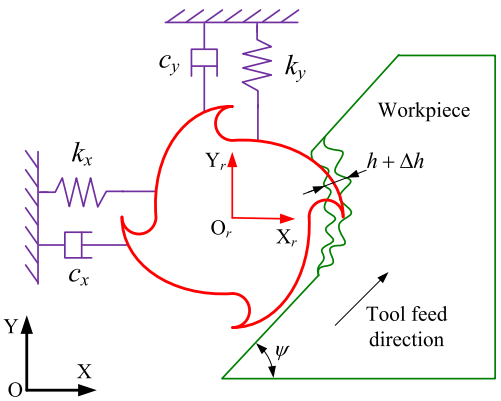

Fig. 3 2-DOF milling dynamics model

Cotes integration formula can be utilized to approximate this initial value problem by

$$\int_{t_i}^{t} \mathbf{G}(t)dt \approx (t - t_k) \sum_{k=0}^{N} \mathbf{G}(t_k) C_k^N \tag{20}$$

where C_k^N is Cotes coefficients.

In order to achieve a high calculation accuracy, let $N = 4$, Eq. 19 is then derived as follows.

$$\begin{aligned}\mathbf{X}(t_{k+4}) = \mathbf{X}(t_k) + \frac{2\tau}{45}(7\mathbf{G}(t_k) + 32\mathbf{G}(t_{k+1}) + 12\mathbf{G}(t_{k+2}) \\ +32\mathbf{G}(t_{k+3}) + 7\mathbf{G}(t_{k+4}))\end{aligned} \tag{21}$$

Substituting $\mathbf{G}(t_k)$, $\mathbf{G}(t_{k+1})$, $\mathbf{G}(t_{k+2})$, $\mathbf{G}(t_{k+3})$, and $\mathbf{G}(t_{k+4})$ into Eq. 21, we can obtain

$$\begin{aligned}&\left[\mathbf{I} - \frac{14\tau}{45}\mathbf{F}_{k+4}\right]\mathbf{X}_{k+4} - \frac{64\tau}{45}\mathbf{F}_{k+3}\mathbf{X}_{k+3} - \frac{8\tau}{15}\mathbf{F}_{k+2}\mathbf{X}_{k+2} \\ &\quad -\frac{64\tau}{45}\mathbf{F}_{k+1}\mathbf{X}_{k+1} - \left[\mathbf{I} + \frac{14\tau}{45}\mathbf{F}_k\right]\mathbf{X}_k \\ &= \frac{14\tau}{45}\{\mathbf{B}_{k+4}\mathbf{X}(t_{k+4} - \bar{\tau}(t_{k+4})) + \mathbf{C}_{k+4}\} \\ &\quad +\frac{64\tau}{45}\{\mathbf{B}_{k+3}\mathbf{X}(t_{k+3} - \bar{\tau}(t_{k+3})) + \mathbf{C}_{k+3}\} \\ &\quad +\frac{8\tau}{15}\{\mathbf{B}_{k+2}\mathbf{X}(t_{k+2} - \bar{\tau}(t_{k+2})) + \mathbf{C}_{k+2}\} \\ &\quad +\frac{64\tau}{45}\{\mathbf{B}_{k+1}\mathbf{X}(t_{k+1} - \bar{\tau}(t_{k+1})) + \mathbf{C}_{k+1}\} \\ &\quad +\frac{14\tau}{45}\{\mathbf{B}_k\mathbf{X}(t_k - \bar{\tau}(t_k)) + \mathbf{C}_k\}\end{aligned} \tag{22}$$

After time discretization at each time interval, $\mathbf{X}(t-\bar{\tau}(t))$ can be approximated by linear interpolation. For $\mathbf{X}(t_{k+s} - \bar{\tau}(t_{k+s}))$ $(s = 0, 1, .., 4)$, using interpolation method, we can get

$$\begin{aligned}\mathbf{X}(t_{k+s} - \bar{\tau}(t_{k+s})) = w_{s,l}\mathbf{X}_{k+s-r_{k+s}} \\ +w_{s,l+1}\mathbf{X}t_{k+s-r_{k+s}-1} \ (s = 0, 1, .., 4)\end{aligned} \tag{23}$$

where $r_{k+s} = \text{int}(\bar{\tau}(t_{k+s})/\tau)$.

$w_{s,l}$ and $w_{s,l+1}$ are the interpolation coefficients, its value can be obtained by

$$\begin{aligned}w_{s,l} &= \begin{cases}(\tau - \tau_0)/\tau & (l = r_{k+s} + 4) \\ 0 & otherwise\end{cases} \\ w_{s,l+1} &= \begin{cases}\tau_0/\tau & (l = r_{k+s} + 5) \\ 0 & otherwise\end{cases}\end{aligned} \tag{24}$$

where $\tau_0 = \tau_{i,j}(t_{k+s}) - r_{k+s} \cdot \tau$.

Now, Eq. 22 can be further derived as

$$\mathbf{X}_{k+4} = \sum_{l=1}^{4+m} \mathbf{E}_{1,l}\mathbf{X}_{k+4-l} + \sum_{s=0}^{4} \mathbf{G}_{k+s}\mathbf{C}_{k+s} \tag{25}$$

where

$$\begin{aligned}\mathbf{E}_{1,1} &= \frac{64\tau}{45}\left[\mathbf{I} - \frac{14\tau}{45}\mathbf{F}_{k+4}\right]^{-1}\mathbf{F}_{k+3} \\ \mathbf{E}_{1,2} &= \frac{8\tau}{15}\left[\mathbf{I} - \frac{14\tau}{45}\mathbf{F}_{k+4}\right]^{-1}\mathbf{F}_{k+2} \\ \mathbf{E}_{1,3} &= \frac{64\tau}{45}\left[\mathbf{I} - \frac{14\tau}{45}\mathbf{F}_{k+4}\right]^{-1}\mathbf{F}_{k+1} \\ \mathbf{E}_{1,4} &= \left[\mathbf{I} - \frac{14\tau}{45}\mathbf{F}_{k+4}\right]^{-1}\left[\mathbf{I} + \frac{14\tau}{45}\mathbf{F}_k\right] \\ \mathbf{E}_{1,l} &= w_{0,l}\frac{14\tau}{45}\mathbf{B}_k + w_{1,l}\frac{64\tau}{45}\mathbf{B}_{k+1} + w_{2,l}\frac{8\tau}{15}\mathbf{B}_{k+2} \\ &\quad +w_{3,l}\frac{64\tau}{45}\mathbf{B}_{k+3} + w_{4,l}\frac{14\tau}{45}\mathbf{B}_{k+4} \ (l = 5, 6, ..., 4+m) \\ \mathbf{G}_{1,1} &= \frac{14\tau}{45}\left[\mathbf{I} - \frac{14\tau}{45}\mathbf{F}_{k+4}\right]^{-1}, \mathbf{G}_{1,2} = \frac{64\tau}{45}\left[\mathbf{I} - \frac{14\tau}{45}\mathbf{F}_{k+4}\right]^{-1}, \\ \mathbf{G}_{1,3} &= \frac{8\tau}{15}\left[\mathbf{I} - \frac{14\tau}{45}\mathbf{F}_{k+4}\right]^{-1}, \\ \mathbf{G}_{1,4} &= \frac{64\tau}{45}\left[\mathbf{I} - \frac{14\tau}{45}\mathbf{F}_{k+4}\right]^{-1}, \mathbf{G}_{1,5} = \frac{14\tau}{45}\left[\mathbf{I} - \frac{14\tau}{45}\mathbf{F}_{k+4}\right]^{-1}\end{aligned}$$

Based on Eq. 25, using the expanded state vector $\mathbf{y}_k = \text{col}(\mathbf{X}_{k+3}, \mathbf{X}_{k+2}, ..., \mathbf{X}_{k-m})$, a discrete map can be defined as

$$\mathbf{y}_{k+1} = \mathbf{E}_k\mathbf{y}_k + \mathbf{G}_k\mathbf{C}_k \tag{26}$$

where

$$\mathbf{E}_k = \begin{bmatrix}\mathbf{E}_{1,1} & \cdots & \mathbf{E}_{1,m+3} & \mathbf{E}_{1,m+4} \\ \mathbf{I} & \cdots & \mathbf{O} & \mathbf{O} \\ \vdots & \ddots & \vdots & \vdots \\ \mathbf{O} & \cdots & \mathbf{I} & \mathbf{O}\end{bmatrix}$$

$$\mathbf{G}_k = \begin{bmatrix}\mathbf{G}_{1,1} & \cdots & \mathbf{G}_{1,5} & \mathbf{O} \\ \mathbf{O} & \cdots & \mathbf{O} & \mathbf{O} \\ \vdots & \ddots & \vdots & \vdots \\ \mathbf{O} & \cdots & \mathbf{O} & \mathbf{O}\end{bmatrix}$$

And the state transition relationship for one period of the system is shown as

$$\mathbf{y}_m = \Phi\mathbf{y}_0 + \mathbf{G} \tag{27}$$

where

$$\Phi = \mathbf{E}_{k-1}\mathbf{E}_{k-2}...\mathbf{E}_1\mathbf{E}_0$$

$$\mathbf{G} = \mathbf{G}_{m-1}\mathbf{C}_{m-1} + \sum_{i=0}^{m-2} \mathbf{E}_{m-1}...\mathbf{E}_{m+i}\mathbf{G}_i\mathbf{C}_i$$

According to Floquet theory [22], the stability of the system can be determined: if the moduluses of all the eigenvalues of the transition matrix Φ are less than unity, the system is stable; otherwise, it is unstable. When the milling system is stable, the steady state response can be achieved from the fixed points as

$$\mathbf{y}* = (\mathbf{I} - \Phi)^{-1}\mathbf{G} \tag{28}$$

Table 1 Milling process parameters

Modal parameters	Direction	Modal mass (kg)	Damping ratio	Modal stiffness (N/m)
	X	0.468	0.037	8.138×10^6
	Y	0.511	0.031	8.647×10^6
Cutting force coefficients	k_t (N/mm^2)		k_r (N/mm^2)	
	840		568	
Cutter runout parameters	ρ (μm)		λ (°)	
	13.3		26.2	

The actual surface profile can be obtained by subtracting the tooth envelope from workpiece, expressed as $S_{surf}(x_u, z_v)$. Then the SLE, which represents the deviation between the actual surface profile S^d_{surf} and the desired surface profile , can be calculated by

$$\mathrm{SLE} = \bar{S}_{surf}(x_u, z_v) - S^d_{surf} \tag{29}$$

3 Verification

In this section, two verification cases are illustrated to test the accuracy and the efficiency of the proposed method. The first one is to compare convergence rate of the proposed stability prediction without cutter runout with other stability prediction methods. Computer programs of the proposed approach are all written in MATLABs 7.10 and run on the same personal computer. The second one is to examine the prediction accuracy of the proposed method in milling process with cutter runout through experiments. The dynamic parameters of tool system are obtained by impact testing as shown in Table 1. These verification cases are carried out by down milling with a three teeth cylindrical end cutter with a diameter of 10 mm and a helix angle of 30°. The material of workpiece is aluminium alloy 7075-T651. Besides, cutting force coefficients and cutter runout parameters can be achieved by calibration experiments which are also illustrated in Table 1. The feed directional angle ψ is set as zero, which namely the cutter feeds along in X the direction. The experimental setup is shown in Fig. 4.

3.1 Numerical verification

The rate of convergence is one of the most important parameters for high performance arithmetic. Just as literatures, the local discretization errors of the SDM with zero-order and first-order SDM are $o(\tau^2)$ [12] and $o(\tau^3)$ [13], respectively, and the local discretization errors of the FDM with first-order, second-order, and third-order are $o(\tau^2)$ [14], $o(\tau^3)$ [15], and $o(\tau^4)$ [16], respectively. Meanwhile, the local discretization error of Zhang's numerical integral methods (NIM) is $o(\tau^5)$ [18]. For the proposed method using the Cotes integration formula, its local discretization error is $o(\tau^7)$, higher than all above mentioned methods. In order to illustrate the rate of convergence more clearly, a 2-DOF milling system with dynamic parameters listed in Table 1 is applied here, the machining parameters are chosen as: aD = 0.5, Ω = 5000 rpm, down milling with two different depth of cut as a_p = 2 and 0.5 mm, respectively. Figure 5 demonstrates the convergence of the critical eigenvalues with respect to different time interval m for the zero-order SDM, the first-order SDM, the first-order FDM, the third-order FDM, the Zhang's NIM, and the proposed method. In Fig. 5, the differences of the approximate modulus of the critical eigenvalue $|\mu|$ and the exact one $|\mu_0|$ are presented as the function of the computational parameter m, where $|\mu_0|$ is determined by using the first-order SDM with m = 400. The results show that the proposed method converges faster than others and it means that the presented method need less time interval with the same local discretization error compared with the literatures methods.

In order to illustrate the accuracy of the presented method, we take the 2-DOF dynamic system as an example to predict stability lobes compared with the zero-order SDM, the second-order FDM, and the Zhangs NIM. The stability lobe computed by first-order SDM with m = 400 is

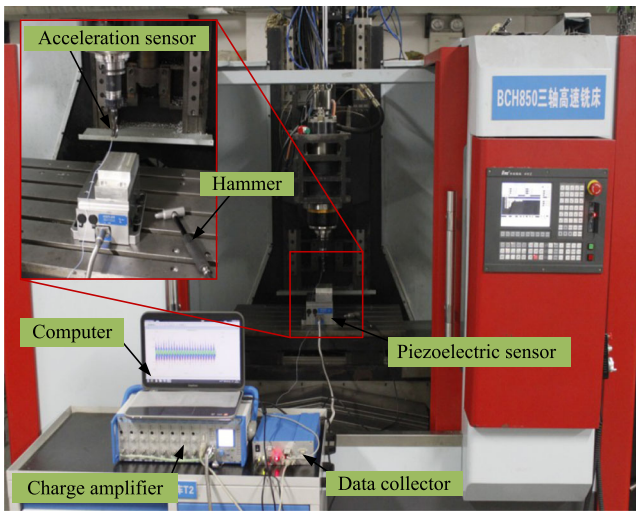

Fig. 4 Experimental setup

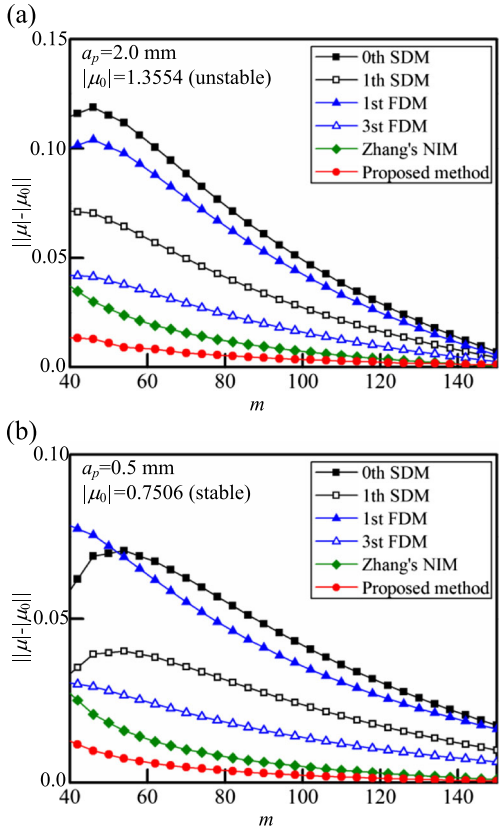

Fig. 5 Convergence of the critical eigenvalues with respect to m using different methods

taken as the exact lobe of the dynamic system. This stability lobe is utilized to be compared with the presented method and other methods with three different time intervals of 20, 60, and 100. The stability prediction results and time consuming are both shown in Fig. 6. The stability charts are calculated over 200 × 100 sized grid on the square with the boundaries of the rotational speed $n \in [3000, 8000]$ rpm and the axial depth of cut $a_p \in [0, 8]$ mm. In the aspect of calculation accuracy, the stability lobes predicted by the proposed method is more rapidly close to the exact stability limit than other methods with the same number of time interval. It indicates that the presented method is feasible and can be taken as an alternative for accurately predicting stability lobes with small number of time interval. In the aspect of time consuming, it can be seen that the runtime of the zero-order SDM with $m = 20$, 60, and 100 are 42.7, 98.8, and 161.4 s, respectively. For the second-order FDM, its corresponding runtime are 33.5, 70.5, and 130.9 s. For the Zhangs NIM, its runtime are 20.7, 43.7, and 81.3 s and the proposed method takes about 24.5, 50.1, and 96.6 s. It can be concluded that the runtime of the proposed method is not obviously increase than the Zhangs NIM, and what should be pointed out is that since matrix exponentials is avoided in this method, its runtime is remarkably decrease compared with the zero-order SDM and the second-order FDM. The decrease percent can reach about 40.1 and 26.2 %, respectively, with m =100.

3.2 Experimental verification

For the experimental verification in this section, the paper firstly predicts the stability in the milling case without cutter runout, and compares it with stability without taking cutter runout into account. As shown in Fig. 7a, a lobe upward shift phenomenon is found for the stability with cutter runout effect ($\rho = 13.3$ μm, $\lambda = 26.2°$) compared with no cutter runout case. Then, a series of milling experiments are further performed. The instantaneous cutting forces are measured by a Kistler 9265B dynamometer. The milling force component in the Y_f direction is transformed by FFT, and then the frequency characteristic is used to judge the occurrence of chatter or not. The analysis results are also plotted in Fig. 7a. It can be seen that experimental results have a good agreement with the prediction stability diagram with cutter runout effect. Meanwhile, the prediction result neglecting cutter runout fails to match the experiments in some local regions because there is an evident distinction between measured data and predicted one. The above analysis indicates that the proposed method can reach a high accuracy for stability prediction.

As shown in Fig. 7b, we further study the milling force frequency characteristic and formed surface topography for four specified cases. The four different cutting conditions are defined as test A ($n = 6450$ rpm, $a_p = 3.2$ mm), B ($n = 6850$ rpm, $a_p = 3.2$ mm), C ($n = 12,900$ rpm, $a_p = 6.5$ mm), and D ($n = 13,300$ rpm, $a_p = 6.5$ mm), which are corresponding with Fig. 7a. The results show that the simulated milling force frequency characteristic agree closely with the measured one in magnitude. In tests A and C, except the tooth pass frequency, there has a remarkable chatter frequency near the main modal of tool system, which reveals that the milling process has occurred quasi-periodic bifurcation. We can also obtain the same conclusion from the obvious surface topography fluctuation in simulation and experiment. However, the frequency characteristic in tests B and D only has tooth pass frequency, and the simulated surface topography is regular, so the milling process is stable. Besides, the simulated SLE in stable milling cases is compared with the experimental one. The contour profile of the workpiece surface is measured by a non-sphere contour measuring instrument PGI. The simulated and experimental SLE are −39.2 and −44.6 μm, respectively, for test B, and are 184.7 and 169.4 μm, respectively, for test D. It can be concluded that there exist a little distinction between the simulated data and the experimental one and the proposed method can ensure the accuracy for SLE prediction.

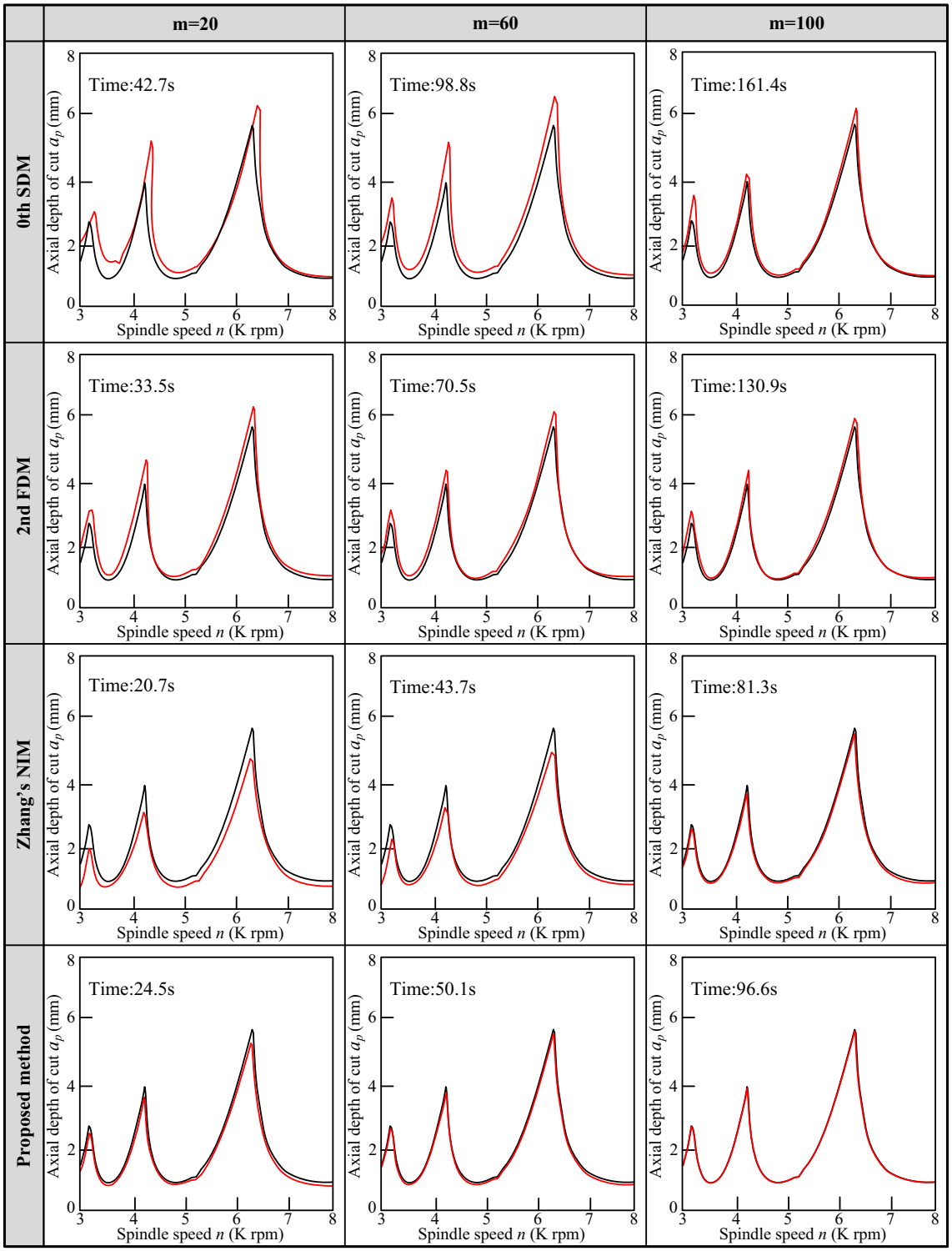

Fig. 6 Stability prediction using different methods with time interval number m of 20, 60, and 100

4 Stability and SLE analysis under different cutting conditions

Based on the above prediction method, the paper numerically analyzes the stability and SLE under different milling conditions in this section. The influence factor includes milling parameters, cutter runout parameters, cutter geometrical parameters, and dynamics of asymmetrical tool system. All analysis are conducted in this section with the same cutter and dynamic system in previous test.

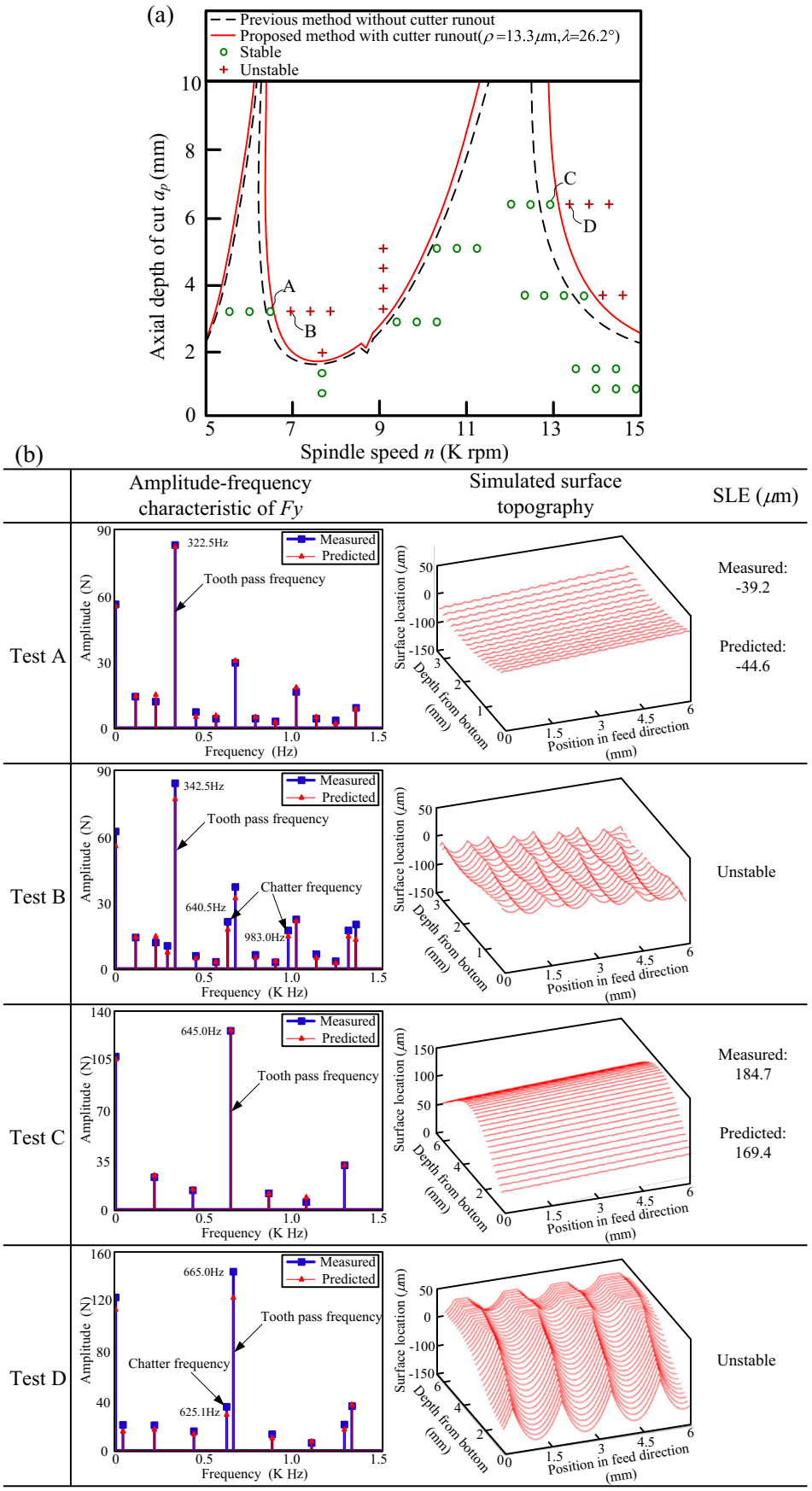

Fig. 7 Experimental verification for milling stability and SLE

4.1 Influence of milling parameters

During the milling process without cutter runout, all teeth can participate into cutting with the same cutting state. As shown in Fig. 8, the milling stability and SLE are illustrated with different feed per tooth f_t during down milling. The feed per tooth f_t are set to 0.05, 0.25, and 0.5 mm/tooth, respectively, and the radial immersion aD is 0.3. Figure 8a shows the stability varies with different feed per tooth and there exist a lobe rightward shift phenomenon. This conclusion differ from the traditional result where the feed per tooth has no effect on stability. But according to the analysis of tool motion during cutter/workpiece engagement in Section 2, the time delay item is larger than that in traditional dynamic model during down milling. The bigger the feed per tooth is, the larger of this deviation. At last, the stability diagram shifts to high spindle speed direction to obtain a uniform time delay for ensuring the same critical axial depth of cut. For SLE in Fig. 8b, a large feed per tooth will generate a high milling force, resulting in a big SLE at the same spindle speed. Besides, the SLE is obviously dependent on spindle speed, when tooth pass frequency is equal to the natural frequency of the tool system, e.g., n = 13,000 or 6500 rpm, the one and two times harmonics of the tooth pass frequency is near to the natural frequency of the tool system, then the milling process will resonate which lead to a large SLE and a poor machining accuracy. Moreover, the dynamical response at some local spindle speed in down milling process produce a negative value of SLE, which indicates over-cut on workpiece surface. In practice, a negative SLE is more undesirable than a positive one, so it is important for a suitable spindle speed selecting.

Figure 9 shows the effect variation of milling type and radial immersion on stability and SLE. The radial immersion aD is set as 0.1, 0.5, and 0.9 mm for both down and up milling. The feed per tooth f_t is 0.1 mm/tooth. It can be seen from Fig. 9a that there is a distinct deviation in stability diagram between down and up milling at low radial immersion milling process, and the stability in down milling is located at right side of that in up milling. Additionally, the deviation gradually disappears with the increase of radial immersion. From the time delay item equation in Section 2, a reasonable explanation for this phenomenon is that the time delay in down milling is bigger than that in up milling, and this disparity is remarkable at low radial immersion milling,

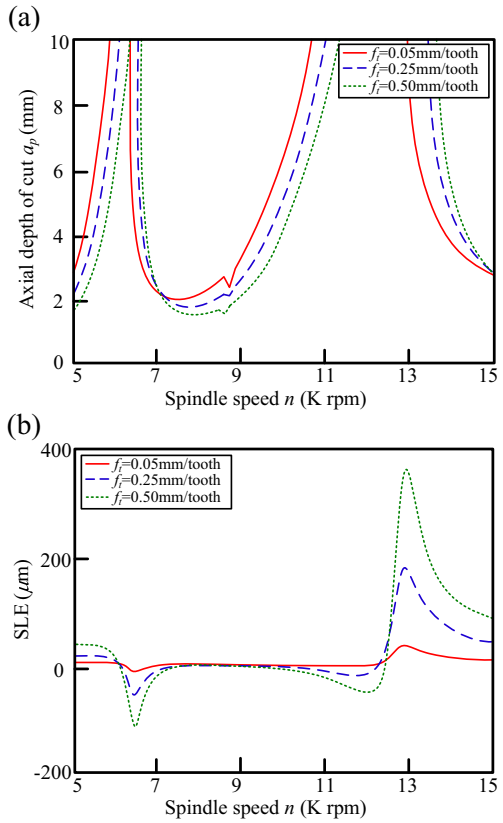

Fig. 8 Stability and SLE with different feed per tooth, aD = 0.3. **a** Stability. **b** SLE, a_p = 1 mm

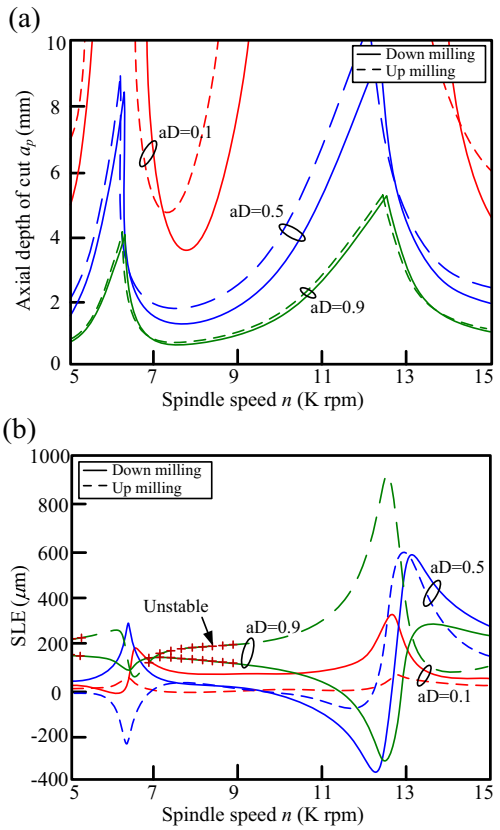

Fig. 9 Stability and SLE with different milling types and radial immersion, aD = 0.3, f_t = 0.1 mm/tooth. **a** Stability. **b** SLE, a_p = 1 mm

but fades away at high radial immersion milling. Moreover, Fig. 9b shows the milling types and radial immersion have an important influence on SLE and these quantitative analysis can provide a theory basis to choose reasonable milling parameters.

4.2 Influence of cutter runout

For the milling case with cutter runout effect, the actual tooth radius changes from its desired one, then the instantaneous chip thickness and time delay item also varies as a result. Besides, the cutting state for all teeth are not same with each other. When cutter runout value is large, some teeth maybe lost of cut. Withal, the cutting state for all teeth will be different with different feed per tooth and radial immersion. For different cutter runout values during down milling, Fig. 10 shows the critical cutting state for all teeth with the combination of feed per tooth and radial immersion. Taking runout value of 20 μm and runout angle of 0° as an example, the whole milling parameters region is divided into three parts, the above one indicates all three teeth are in cut, the middle one indicates only two teeth are in cut, and the bottom one indicates only one tooth is in cut. The teeth tends to lost of cut in low radial immersion milling case. For different cutter runout values, the cutting state region will change. During the increase of cutter runout value, the three teeth cutting region would minish, and the one tooth cutting region would augment.

Figure 11 shows the variation of stability and SLE affected by cutter runout parameters. The radial immersion aD is 0.3 during down milling and the feed per tooth f_t is 0.03 mm/tooth. As seen in Fig. 11a, the stability diagram changes evidently when runout value increases from 0 to 40 μm with runout angle of zero. For the milling case with small runout value, the cutting state for all teeth are in-cut, the stability diagram has little change at some local region,

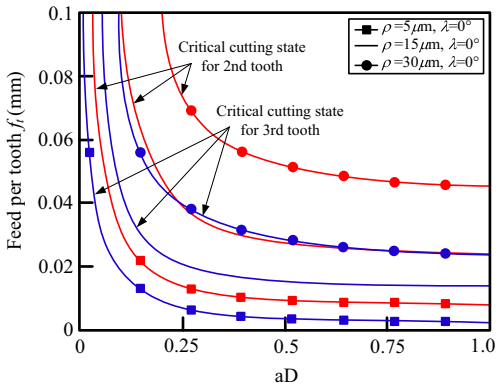

Fig. 10 Critical cutting state for all teeth under the combination of feed per tooth and radial immersion with different cutter runout parameters

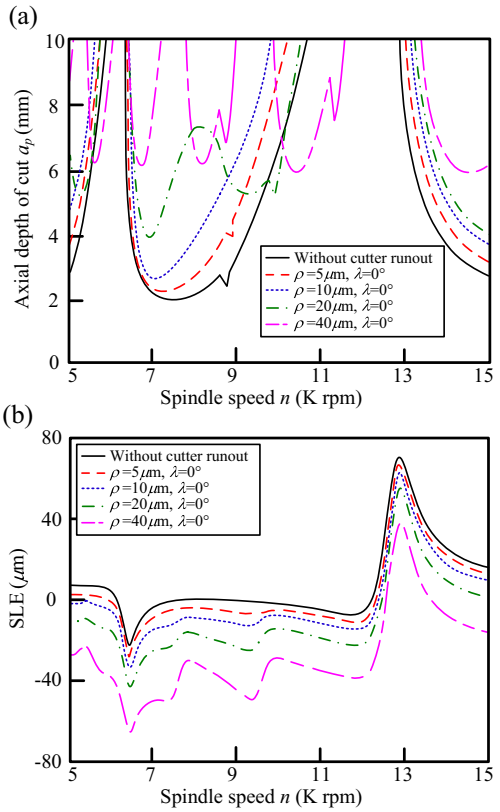

Fig. 11 Stability and SLE with different cutter runout parameters, aD =0.3, f_t = 0.03 mm/tooth. **a** Stability. **b** SLE, a_p = 1 mm

and the stability topology is invariant. When the runout value increases to 20 μm, it can be deduced that only two teeth are in-cut based on Fig. 10, then its incentive mechanism of the dynamic system is not same with that in milling case with small runout value, which results in the change of stability topology. For a large runout value of 40 μm, only one tooth is in-cut in this milling condition, thus the stability topology change entirely. It can be concluded that cutter runout will disturb the incentive mechanism of milling process, and the lager the runout value is, the higher of critical axial depth of cut, then which results in the lobe upward shift phenomenon. Figure 11b details the variation of SLE under different cutter runout value. It is observed that the over-cut phenomenon increases evidently with the increase of runout value. Moreover, cutter runout would arouse some new incentive frequency for milling forces, e.g., the fundamental frequency of spindle speed and its high order harmonics, the accuracy of formed surface will deteriorate when these harmonics induce system resonance. As shown in Fig. 10b, when spindle speed is 9750 and 7500 rpm, the 4 and 5 times harmonics of spindle rotation frequency coincide with the natural frequency of the tool system, then we can see the SLE increase rapidly.

4.3 Influence of cutter geometrical parameters

Figure 12 shows the simulation results of stability and SLE corresponding to three different tooth helix angle β, e.g., 0°, 15°, and 30°. The influence of radial immersion is synthetically considered here. The radial immersion aD is set as 0.05 and 0.5, respectively, and the feed per tooth f_t is 0.1 mm/tooth during down milling operation. In order to analyze conveniently, the boundary of axial depth of cut is preset as [0,100] mm. As plotted in Fig. 12a, it can be seen that the period doubling lobe appears when the tooth helix angle is zero, but it disappears when tooth helix angle equals to 15° and 30°. Some milling experiment cases have been conducted to verify the milling stability with tooth helix angle of 0°. As helix angle would affect cutting force coefficients, and the local stability shows a disagreement trend between experiment and simulation. Regardless of this reason, the whole comparison results reveal that predictive capability of the proposed method with different helix angle. For the milling case with large radial immersion, the influence of tooth helix on stability is weak. The reason for this consequence is that the stability diagram is low in this milling condition which results in an insignificant impact of tooth helix angle. Figure 12b analyzes the SLE under two different milling parameters (caes 1: aD = 0.05, a_p = 10 mm; caes 2: aD = 0.5, a_p = 1 mm). Since large tooth helix angle is more avail for cutter/workpiece engagement during tooth entry and exit stage, which can decrease cutter response. As seen from Fig. 12b, the larger the tooth helix angle is, the smaller the SLE is, especially for the resonance region for both milling cases with large or low radial immersion.

Figure 13 gives the stability and SLE for nonconstant pitch cutter. The pitch angle for the three teeth cutter is $120° - \Delta\theta \sim 120 \sim 120° + \Delta\theta$. In the milling simulation, the radial immersion aD is 0.3 and the feed per tooth f_t is 0.1 mm/tooth. When the pitch angle variable is set to 20° and 40°, the stability changes evidently compared with constant pitch cutter. Furthermore, the SLE for nonconstant pitch cutter is more complex. This result can be attributed to the intricate incentive mechanism in milling process with nonconstant pitch cutter.

4.4 Influence of dynamics parameters in asymmetrical tool system

In practice, as the various structure of tool system, the dynamics in the X and Y directions maybe different. The

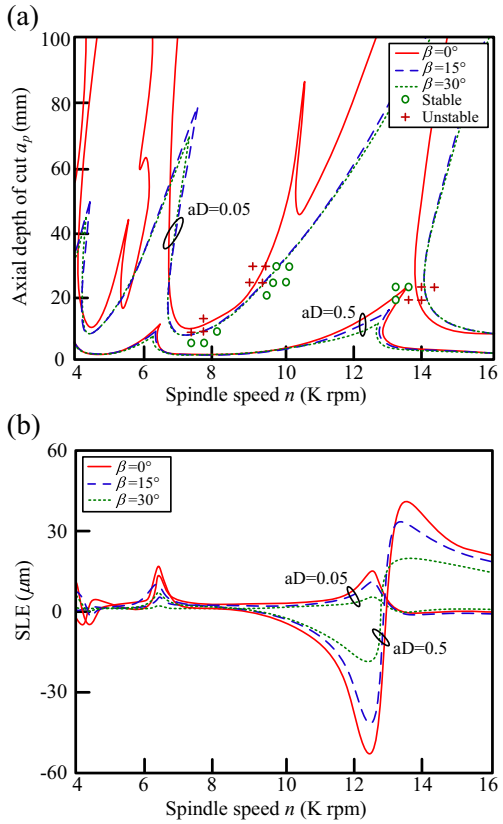

Fig. 12 Stability and SLE with different tooth helix angle, f_t = 0.1 mm/tooth. **a** Stability. **b** SLE, aD = 0.05 with a_p = 10 mm, aD = 0.5 with a_p = 1 mm

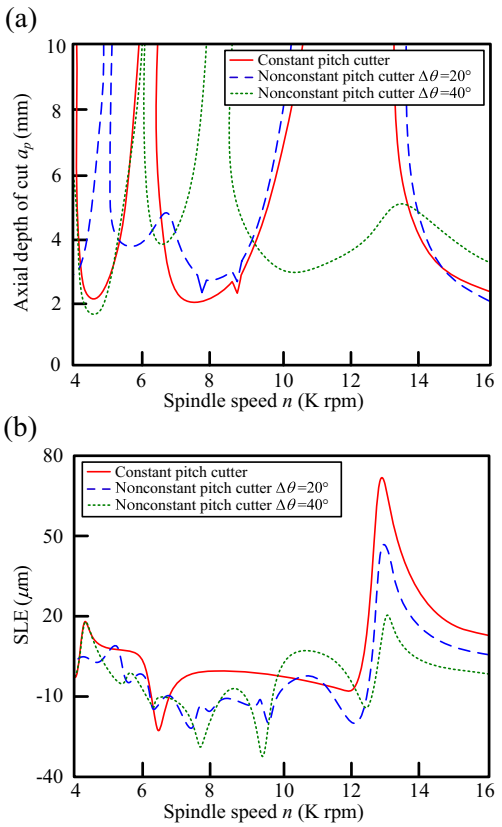

Fig. 13 Stability and SLE with different pitch angle, aD = 0.3, f_t = 0.1 mm/tooth. **a** Stability. **b** SLE, a_p = 1 mm

modal parameters of this orthogonal axis can affect the milling stability and SLE, and the influence is different under different tool feed directional angle. For comparison, here the paper only analyzes minimum critical axial depth of cut and maximum SLE. The radial immersion aD is 0.3 and the feed per tooth f_t is 0.1 mm/tooth.

In this study, the boundary of feed directional angle is set as $\psi \in [0°, 360°]$. The asymmetrical percent of modal mass, stiffness, and damping are all equivalent to 20 %. The minimum critical axial depth of cut of the milling system are shown in Fig. 14a, c, e, and the maximum SLE are shown in Fig. 14b, d, f.

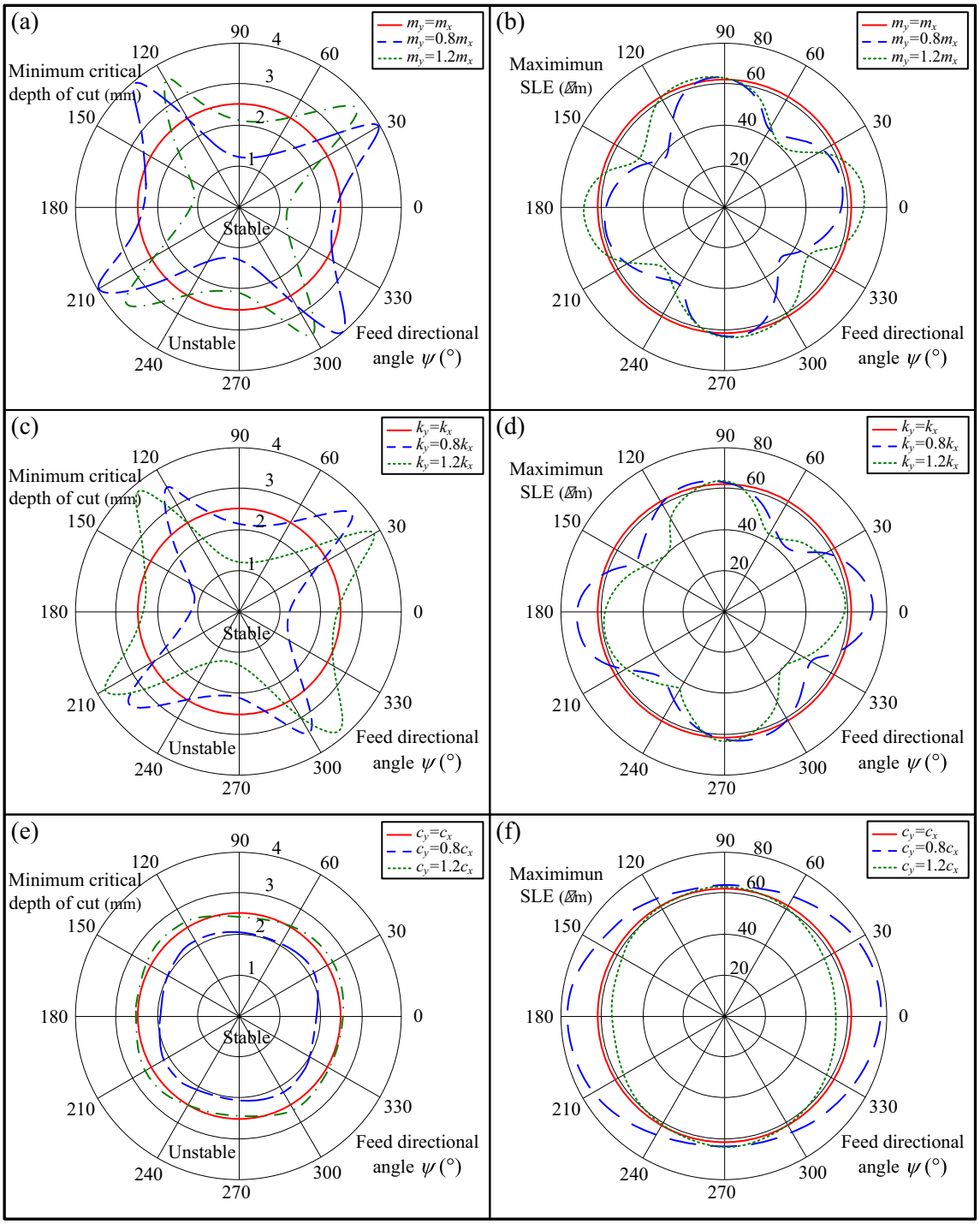

Fig. 14 Stability and SLE under asymmetrical tool system, aD = 0.3, f_t = 0.1 mm/tooth. **a**, **c**, **e** Stability. **b**, **d**, **f** SLE, a_p = 1 mm

Taking asymmetrical modal mass as an example, as seen from Fig. 14a, b, both minimum critical axial depth of cut and maximum SLE of a symmetrical system are circle curves with different feed directional angles, which means that feed direction has no effect on milling process for symmetrical system. When the modal mass in the Y direction is bigger or smaller than X direction with 20 %, the minimum critical axial depth of cut and maximum SLE are irregular diagram with multi-extremum. For the case with $m_y = 0.8m_x$, the minimum critical axial depth of cut would reach its local maximum at $\psi = 30°, 130°, 210°, 310°$ and local minimum at $\psi = 85°, 175°, 265°, 355°$, and the local maximum is about three times of local minimum. Meanwhile, the maximum SLE would reach its local maximum at $\psi = 12°, 96°, 192°, 276°$ and its local minimum at $\psi = 60°, 140°, 240°, 320°$, and the local maximum is about 1.5 times of its local minimum. For the case with $m_y = 1.2m_x$, the distribution topology of minimum critical axial depth of cut and maximum SLE is a result of rotating and scaling of the milling case with $m_y = 0.8m_x$.

The results of asymmetrical modal stiffness are shown in Fig. 14c, d. As the influence of modal stiffness and mass on natural frequency are contrary, so we can see that the influence variation of minimum critical axial depth of cut and maximum SLE for asymmetrical modal stiffness is opposite to the milling case with asymmetrical modal mass. Besides, the effect of asymmetrical modal damping on the minimum critical axial depth of cut and maximum SLE is given in Fig. 14e, f. The curve distribution topology is similar to an ellipse. Contrasting to modal mass and stiffness, the modal damping affect milling dynamics is more slight thus its variation tendency is more gentle. The above analysis indicates that the stability and SLE have close relationship with the asymmetrical tool system, and the feed direction has an important influence on machining performance. So, the study in this section can provide a theoretical guide for feed direction selection in an asymmetrical dynamic milling system.

5 Conclusion

This paper presents an efficient approach for milling stability and SLE prediction with varying time delay and cutter runout effect, which is validated by numerical and experimental cases, and the efficiency and accuracy are ensured. The stability and SLE under different milling conditions, including milling parameters, cutter runout, cutter geometry, and asymmetric milling system, are also studied. The main conclusions are as follows:

(1) The time delay item is a periodic varying variable as a result of tooth trochoid motion, which resulting in the lobe leftward or rightward shift phenomenon. Cutter runout alters the tooth cutting state and lead time delay occur change suddenly, and which can disturb the incentive mechanism of milling process to obtain a higher critical axial depth of cut.

(2) Due to Cotes numerical integration formula, the local discretization error of the proposed stability prediction method is $o(\tau^7)$, which is higher and converging faster than all existing methods. The proposed method for stability and SLE prediction are in good agreement with the experimental results, and have a high accuracy for stability prediction with taking cutter runout and varying time delay into account.

(3) Large cutter runout can lead tooth to lost of cut, and then change the stability topology entirely. Besides, when the excitation frequency of the milling force is equal to the natural frequency of the system, there is a sharp increase for the SLE, and this phenomenon also occurs for the new frequency coming from cutter runout effect.

(4) Under the milling process with asymmetric structure, the minimum critical axial depth of cut and maximum SLE represents multi-extreme variation with feed direction angle, and these extremes would deviate from coordinate axes, which is very important for tool path planning and parameters selection.

Acknowledgments This work was financially supported by the National Natural Science Foundation (No. 51375373), the National High Technology Research and Development Program of China (No. 2013AA041108), and the Key Project of National Natural Science Foundation (No. 51235009).

References

1. Tlusty J (2000) Manufacturing processes and equipment. Prentice Hall, Upper Saddle River
2. Altintas Y (2000) Manufacturing automation. Cambridge University Press, New York
3. Tlusty J, Polacek M (1963) The stability of machine tools against self-excited vibrations in machining. Trans of ASME Int Res in Prod Eng:465–474
4. Tobias SA (1965) Machine tool vibration. Blackie, London
5. Tobias SA, Fishwick W (1958) A theory of regenerative chatter. The Engineer, London
6. Merritt H (1965) Theory of self excited machine tool chatter. Trans ASME J Eng Ind 87(4):447–454
7. Tlusty J, Ismail F (1981) Basic nonlinearity in machining chatter. Annals CIRP 30:299–304
8. Tlusty J, Ismail F (1983) Special aspects of chatter in milling. J Vibration, Acoustics. Stress, and Reliability in Design 105: 24–32
9. Altintas Y, Chan P (1992) In-process detection and suppression of chatter in milling. Int J Mach Tools Manuf 32:329–347
10. Altintas Y, Budak E (1995) Analytical prediction of stability lobes in milling. Annals CIRP 44(1):357–362

11. Merdol SD, Altintas Y (2004) Multi frequency solution of chatter stability for low immersion milling. Trans ASME J Manuf Sci Eng 126(3):459–466
12. Insperger T, Stépán G (2002) Semi-discretization method for delayed systems. Int J Num Meth Eng 55(5):503–518
13. Insperger T, Stépán G, Turi J (2008) On the higher-order semi-discretizations for periodic delayed systems. J Sound and Vibration 313(1-2):334–341
14. Ding Y, Zhu LM, Zhang XJ, Ding H (2010) A full-discretization method for prediction of milling stability. Int J Mach Tools Manuf 50:502–509
15. Ding Y, Zhu LM, Zhang XJ, Ding H (2010) Second-order full-discretization method for milling stability prediction. Int J Mach Tools Manuf 50(2010):926–932
16. Quo Q, Sun YW, Jiang Y (2012) On the accurate calculation of milling stability limits using third-order full-discretization method. Int J Mach Tools Manuf 62:61–66
17. Ding Y, Zhu LM, Zhang XJ, Ding H (2011) Numerical integration method for prediction of milling stability. Trans ASME J Manuf Sci Eng 133(3) 031005
18. Zhang Z, Li HG, Meng G, Liu C (2015) A novel approach for the prediction of the milling stability based on the Simpson method. Int J Mach Tools Manuf 99:43–47
19. Martelloti ME (1941) An analysis of the milling process. Transactions of the ASME 63:677–700
20. Long XH, Balachandran B, Mann BP (2007) Dynamics of milling processes with variable time delays. Nonlinear Dyn 47:49–63
21. Song QH, Liu ZQ, Shi ZY (2014) Chatter stability for micromilling processes with flat end mill. Int J Adv Manuf Technol 71:1159–1174
22. Liang XG, Yao ZQ, Luo L, Hu J (2013) An improved numerical integration method for predicting milling stability with varying time delay. Int J Adv Manuf Technol 68:1967–1976
23. Seguy S, Insperger T, Arnaud L, Dessein G, Peign G (2010) On the stability of high-speed milling with spindle speed variation. Int J Adv Manuf Technol 48:883–895
24. Sellmeier V, Denkena B (2011) Stable islands in the stability chart of milling processes due to unequal tooth pitch. Int J Mach Tools Manuf 51(2):152–164
25. Wan M, Zhang WH, Dang JW, Yang Y (2010) A unied stability prediction method for milling process with multiple delays. Int J Mach Tools Manuf 50:29–41
26. Montgomery D, Altintas Y (1991) Mechanism of cutting force and surface generation in dynamic milling. Trans ASME J Eng Ind 113:160–168
27. Altintas Y, Lee P (1996) A general mechanics and dynamics model for helical end mills. Annals CIRP 45(1):59–64
28. Altintas Y, Engin S (2001) Generalized modeling of mechanics and dynamics of milling cutters. Annals CIRP 50(1):25–30
29. Ismail F, Elbestawi MA, Du R, Urbasik K (1993) Generation of milled surfaces including tool dynamics and wear. Trans ASME J Eng Ind 115:245–252
30. Schmitz TL, Couey J, Marsh E, Mauntler N, Hughes D (2007) Runout effects in milling: surface finish, surface location error, and stability. Int J Mach Tools Manuf 47:841–851
31. Schmitz TL (2009) Machining dynamics frequency response to improved productivity. Springer
32. Surmann T, Enk D (2007) Simulation of milling tool vibration trajectories along changing engagement conditions. Int J Mach Tools Manuf 47:1442–1448
33. Surmann T, Biermann D (2008) The effect of tool vibrations on the flank surface created by peripheral milling. CIRP Annals-Manuf Technol 57(1):375–378